Stochastic modeling of classifying aerodynamic lenses for separation of airborne particles by material and size

Orkun Furat[a,*], Matthias Masuhr[b], Frank Einar Kruis[b], Volker Schmidt[a]

[a]Institute of Stochastics, Ulm University, Helmholtzstr. 18, 89069 Ulm, Germany; [b]Institute of Technology for Nanostructures (NST) and Center for Nanointegration Duisburg-Essen (CENIDE), University of Duisburg-Essen, Bismarckstr.81, 47057 Duisburg, Germany

ARTICLE HISTORY
Compiled January 20, 2020

ABSTRACT
A flexible stochastic approach is described to model separation processes, in which air-borne particles are separated via a setup of one or more aerodynamic lens orifices. Varying the size of the orifices, the focusing pressure and the mass flow rate through the lens, leads to focusing of particles with distinct aerodynamic properties on the central axis. In this modeling approach a bivariate transfer function is used to describe the passage probability of particles depending on their size and mass. The distribution of feed particles and the changes of the distribution due to the separation process is described via probability densities. The modeling procedure is applicable to various kinds of separation methods and allows optimization of geometric and operation parameters. To this end, the model utilizes flexibly defined separation performance measures which are illustrated in a case study that considers the separation of Cu particles from SiO_2 particles. The spherical particles in the considered virtual mixtures are described by their log-normally distributed diameters and their normally distributed mass densities. Furthermore, the cases are selected in such a manner that the mean aerodynamic diameters of both Cu and SiO_2 particles are equal.

KEYWORDS
aerodynamic sizing; material separation; aerosol; stochastic modeling; classifying aerodynamic lens

1. Introduction

The technique of aerodynamic focusing has applications in concentrating particles to a focused beam in low pressure environments (Klimešová et al., 2019), in mass spectrometry (Drewnick et al., 2005; Schreiner et al., 1999) and in synthesizing nanostructured materials (Dong et al., 2004; Piseri et al., 2004). Early works on aerodynamic focusing conclude that it might be the basis for new aerosol measurement techniques (de La Mora and Riesco-Chueca, 1988). Furthermore, Rao et al. (1993) continued investigating the focusing of particles in viscous jets, showing that focusing is possible even when

* Corresponding author. E-mail address: orkun.furat@uni-ulm.de, Phone: +49731/50 23555, *Fax:* +49731/50 23649

the flow conditions are not laminar. Focusing is often achieved by utilizing aerodynamic lenses, consisting of radial symmetrical pipes with an orifice (Liu et al., 1995), into which an aerosol is injected at the center of the pipe's end. Then, the orifice leads to a temporary flow contraction which results in a focused stream of aerosol. Liu et al. (1995) characterized the focusing quality of aerodynamic lenses by a dimensionless contraction factor which in detail describes the features that contribute to the broadening of particle beams. Aerodynamic focusing of particles is the basis for various characterization techniques. For example, Mallina et al. (1999) describe the rapid single-particle mass spectrometry technique, for analyzing the chemical content of ultrafine aerosols, including a particle inlet, which is able to transmit particles of different sizes, by varying the nozzle pressure – a principle that is similar to the approach utilized in the present work. A thorough numerical investigation of particle trajectories in aerodynamic lenses is performed by Zhang et al. (2002). They found that the contraction of a focused particle is highest for Stokes numbers smaller, yet close to one. On the other hand, for larger Stokes numbers, significant impact losses occurred. Wang et al. (2005) propose a procedure for designing aerodynamic focusing lenses for small particles, based on numerical simulations. In their algorithm, design decisions are dictated by the minimum reachable pressure which is introduced by limitations of the available equipment. Then, Wang and McMurry (2006) released a tool for designing aerodynamic lenses for focusing nanoparticles. Therefore, they computed optimal Stokes numbers beforehand via CFD simulations. Later on, as part of a project on multiparameter characterization of aerosols, a new device, namely the Differential Aerodynamic Particle Sizer (DAPS) was described. The DAPS allows to measure the aerodynamic diameter of nanoparticles by focusing various particle sizes in order to investigate specific, nearly monodisperse particle fractions (Babick et al., 2018).

The DAPS is based on the principle of classifying aerodynamic lenses. In contrast to aerodynamic lenses a classifying aerodynamic lens (CAL), see Figure 1, behaves more like a prism than a lens. More specifically, the aerosol is injected at a well-defined radial region offside the center line of the pipe, which results in the separation of particles when passing through the lens due to their distinct relaxation time τ_p. Before passing through the lens the aerosol must follow the contracting streamlines which widen again after the orifice to accommodate the available space. Inertial and drag forces play vital roles here, because a particles path depends on its Stokes number: It either stays on its original streamline, which is the direction determined while passing through the orifice, or it adapts partially or fully to a new streamline. The consequence is that particles possessing a specific relaxation time τ_L, as a result of the flowing conditions and the design of the lens, will be focused on the centerline of the CAL. Lighter and smaller particles will follow the new streamline, while larger, denser particles will not adapt to the new streamline and move towards the walls of the pipe. The portion of the aerosol which is focused on the centerline, however, is collected via an orifice, which we will call the sampler. This separation process results in a transfer function which shows a differential, classifying behavior which motivates the wording "classifying aerodynamic lens". Using this approach, it is possible to yield a "mono-aerodynamic" aerosol. More precisely, a CAL separates particles whose relaxation times τ_p are approximately equal to a characteristic value τ_L, called lens relaxation time, which depends on the CAL's operating parameters. Since a particle's relaxation time τ_p depends on its size d_p and its mass density ρ_p, CALs can be used to achieve separation with respect to multidimensional particle characteristics. Therefore, the present paper introduces a stochastic model, which describes the separation processes of particle mixtures. For any distribution of feed particle characteristics, which can be freely chosen, the model

describes the distribution of product particle characteristics depending on operating parameters. The general approach can be described by the following steps:

(i) Define the governing equations which describe the influence of particle characteristics and operating parameters on the separation process (Section 2.1).
(ii) Describe these relationships stochastically in form of a transfer function which describes the separation probability of a particle based on its physical characteristics (Section 2.2).
(iii) Define the distribution of characteristics of the considered particle mixture (Section 2.3).
(iv) Combine the last two steps into a stochastic model which describes the distribution of particle characteristics after separation in dependence of operating parameters (Section 2.4).
(v) Define the operating parameters to be optimized and their respective physical and technical limitations (Section 2.5).
(vi) Define performance measures suitable for the process which characterize separation process (Section 2.6).
(vii) Apply optimization algorithms to obtain operating parameters which lead to in a reasonable separation in accordance with the performance measures defined in the previous step (Section 3).

These steps can be used to virtually optimize any separation process for which the particle systems and the relationships between particle characteristics, operating parameters and separation probabilities are known. In the present paper, we demonstrate these steps in detail for the separation of particles from an aerosol based on their mass density and size using CALs.

2. Methods

There are several challenges to overcome when setting up a separation experiment based on a classifying aerodynamic lenses. The most important parameters are focusing pressure p, which is the pressure before the orifice, mass flow $\dot{Q}_m$ and the diameter of the CAL orifice d_{L}. Even when the importance of additional details, such as the geometric shape of nozzles and sampler and the radial position of the aerosol inlet, is neglected, the interdependence of pressure p, mass flow $\dot{Q}_m$ and orifice diameter d_{L} creates a complex optimization problem for separation processes. Once a configuration of lens geometry and operating parameters is chosen, the manufacturing and testing of the prototype is costly in time and money. To minimize the risk it is good practice to simulate the separation process, using numerical fluid dynamics and particle trajectory analysis. However, CFD simulations of CALs are difficult, because they make use of critical orifices[1]. These possess high aspect ratios and creating appropriate meshes is an elaborate process. Therefore, there is a need for a fast, reliable prediction method. The present paper utilizes stochastic models for predicting the most promising set-up. For that purpose we propose a stochastic description of CALs, which decorates each vector of particle characteristics with a realistic probability for passing through a lens.

Then, we describe the incoming particle mixtures stochastically with the help of two-dimensional probability distributions for the random vector of particle size and mass density. By combining such probability distributions with the stochastic descrip-

[1] Critical orifices are used to define the mass flow rate into the lens.

tion of CALs we are able to determine the distribution of size and mass density for outgoing particles. Moreover, this approach makes it possible to derive formulas for performance measures, such that fast numerical computation of these performance measures for arbitrary lens parameters and particle mixtures, represented by two-dimensional probability distributions, is possible. Thus, the performance measures can be maximized efficiently for any known particle mixture by finding optimal operating parameters for the CAL.

2.1. Particle and lens relaxation times

A CAL focuses particles of a certain optimal Stokes number on the central axis, where they are collected via a sampling orifice. The optimal Stokes number Stk_o is a function of Mach and Reynolds number, but is usually close to unity, see Wang et al. (2005). In the present paper we make the general assumption that $Stk_\mathrm{o} = 1$. The Stokes number of a particle is calculated by

$$Stk = \frac{\tau_\mathrm{p} u}{\ell}, \tag{1}$$

where ℓ is the diameter of the lens[2], u is the gas velocity and τ_p the particle relaxation time, describing the time a spherical body needs to adapt to changing flow conditions. The particle relaxation time τ_p depends on the particle mass density ρ_p and the volume equivalent diameter d_p, and is given by

$$\tau(d_\mathrm{p}, \rho_\mathrm{p}) = \frac{\rho_\mathrm{p} d_\mathrm{p}^2 C_c(p, d_\mathrm{p})}{18\eta}, \tag{2}$$

where η is the viscosity of the gas, p is the pressure and C_c is the Cunningham correction. Equation (2) is valid for spherical particles. The Cunningham correction describes the quantity of slipping that occurs between particles and gas molecules as a dimensionless factor greater than one. It depends on the particle size and the mean free path of the gas molecules (Friedlander (2000); Willeke (2011)). The mean free path is defined by pressure, thus the particle relaxation time τ_p is via the Cunningham Correction a function of pressure p.

Assuming that the velocity field and the diameter of the orifice are constant, it is deduced that a particle is focused, when its particle relaxation time τ_p equals a lens specific specific relaxation time τ_L. This characteristic value of the lens is given by

$$\tau_\mathrm{L}(d_\mathrm{L}, \dot{Q}_m, p) = \frac{Stk_\mathrm{o} \cdot d_\mathrm{L}}{u} = \frac{Stk_\mathrm{o} \cdot \frac{\pi}{4} d_\mathrm{L}^3 \cdot \rho_\mathrm{g}(p)}{\dot{Q}_m}, \tag{3}$$

where d_L is the diameter of the lens, $\dot{Q}_m$ is the mass flow through it, ρ_g is the gas density at a defined focusing pressure p. In order to focus particles with given size and mass density the characteristic relaxation time of the particle τ_p must be equal to the relaxation time τ_L of particles focused by the lens. Combining Equations (2) and (3)

[2]the length of the relevant dimension of the obstacle

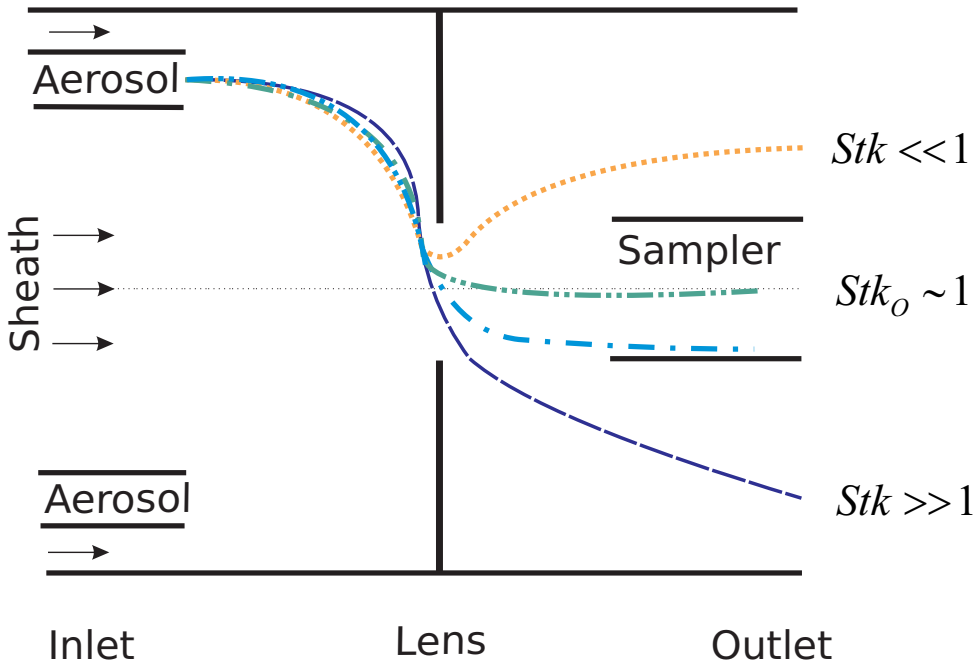

Figure 1. Working principle of a classifying aerodynamic lens (CAL) according to Babick et al. (2018): The aerosol is injected into a stream of sheath gas at a defined radial region. After passing the lens, only particles with Stokes numbers Stk close to $Stk_\mathrm{o} \approx 1$ are collected via the sampler (dash-dotted green or blue line).

the following formula is obtained:

$$d_\mathrm{L} = \left(\frac{2\rho_\mathrm{p} d_\mathrm{p}^2 C_C(p, d_\mathrm{p}) \dot{Q}_m}{9\pi\rho_\mathrm{g}\eta Stk_\mathrm{o}} \right)^{\frac{1}{3}}, \tag{4}$$

where ρ_g is the gas density. Note that for every particle of volume equivalent diameter d_p and mass density ρ_p, there are infinitely many possible combinations of pressure p, mass flow $\dot{Q}_m$ and the lens diameter d_L that focus the particle and thus allow to separate it from particles with deviating diameter or mass density.

There is an additional ambiguity involved: Equation (2) is not bijective, such that there will be cases where particles with distinguishable size and mass density possess equal particle relaxation times and thus the same aerodynamic properties, described by the aerodynamic diameter d_a given by

$$d_\mathrm{a} = d_\mathrm{p}\sqrt{\frac{\rho_\mathrm{p}}{\rho_0}}, \tag{5}$$

where ρ_0 is the unit mass density (Willeke, 2011).

2.2. Transfer functions of CALs

As stated above particles are focused by a CAL if their relaxation time fulfills the following equation:

$$\widetilde{\tau}(d_\mathrm{p}, \rho_\mathrm{p}) = \frac{\tau(d_\mathrm{p}, \rho_\mathrm{p})}{\tau_\mathrm{L}} = 1. \tag{6}$$

We call $\widetilde{\tau}(d_\mathrm{p}, \rho_\mathrm{p})$ the normalized relaxation time of the particle. The set of configurations $\{(d_\mathrm{p}, \rho_\mathrm{p}) \in \mathbb{R}^2_+ \colon \widetilde{\tau}(d_\mathrm{p}, \rho_\mathrm{p}) = 1\}$ form a curve in the two-dimensional parameter space of particle sizes and mass densities. These so-called iso-τ lines are visualized in Figure 2a for three different pressures p. The other two lens parameters $\dot{Q}_m$ and d_L are kept constant in the visualized three scenarios. An "optimal" lens would solely separate particles for which the tuples $(d_\mathrm{p}, \rho_\mathrm{p})$ belong to the CAL's iso-τ line, i.e., which fulfill Equation (6). However, particles with $\widetilde{\tau}(d_\mathrm{p}, \rho_\mathrm{p})$ values close to 1 can be separated with some probability. To model this, we define a trapezoidal transfer function $\Omega \colon (0, \infty) \to [0, 1]$ by

$$\Omega(\widetilde{\tau}) = \frac{1}{2\beta(1-\delta)} \big(|\widetilde{\tau} - (1+\beta)| + |\widetilde{\tau} - (1-\beta)| - |\widetilde{\tau} - (1+\beta\delta)| - |\widetilde{\tau} - (1-\beta\delta)| \big), \tag{7}$$

where β, δ are model parameters. In general, the shape of the transfer function depends on the separation process. The transfer function Ω given in Equation (7) is taken from Stolzenburg and McMurry (2008), where it is used to describe the behavior of differential mobility analyzers. In particular, the trapezoidal shape of Ω fits the transfer function obtained by numerical simulations of particle trajectories through a CAL reported by Babick et al. (2018). More details on the procedure of obtaining the transfer behavior through numerical simulations are described in Kiesler et al. (2019). Alternatively, it can be obtained experimentally, e.g., by measuring the concentration of a mono-disperse aerosol before and after separation, while varying the particle size. The transfer function Ω given by Equation (7) allows to mimic the general form of the transfer behavior of CALs. Figure 2b shows such a transfer function Ω with parameters $\beta = 0.4$ and $\delta = -0.25$. The value of $\Omega(\widetilde{\tau})$ describes the probability that a particle with normalized relaxation time $\widetilde{\tau}$ passes through the CAL. Furthermore, the transfer function Ω is symmetrical around $\widetilde{\tau} = 1$, while the parameter β controls the width of the trapezoid transfer function. For wider transfer functions particles with $\widetilde{\tau}$ values different from 1 can pass through the lens more easily. The parameter δ influences the height of the trapezoid, which influences how likely particles with normalized relaxation times $\widetilde{\tau} = 1$ pass through the lens.

In order to obtain a particle size and mass density dependent transfer function T_L of a CAL with relaxation time τ_L and particle relaxation time dependent transfer function Ω, we combine Equations (6) and (7). This leads to the bivariate transfer function $T_\mathrm{L} \colon (0, \infty)^2 \to [0, 1]$ of a CAL given by

$$T_\mathrm{L}\left(d_\mathrm{p}, \rho_\mathrm{p}\right) = \Omega\left(\widetilde{\tau}(d_\mathrm{p}, \rho_\mathrm{p})\right) = \Omega\left(\frac{\tau(d_\mathrm{p}, \rho_\mathrm{p})}{\tau_\mathrm{L}}\right). \tag{8}$$

The value of $T_\mathrm{L}(d_\mathrm{p}, \rho_\mathrm{p})$ is the probability that a particle with size d_p and mass density ρ_p passes through the lens, see Figure 2c. It can be considered as a two-dimensional transfer function which describes the separation behavior of a CAL with respect to particle size and mass density.

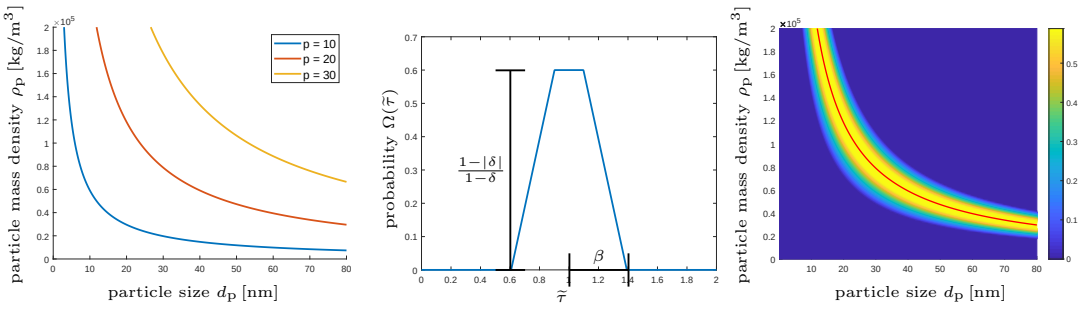

Figure 2. a) Iso-τ lines in the $(d_\mathrm{p}, \rho_\mathrm{p})$ plane for different pressures p with constant lens diameter $d_\mathrm{L} = 0.008\,\mathrm{m}$ and equivalent mass flow $\dot{Q}_\mathrm{slm} = 0.001\,\mathrm{slm}$. b) Transfer function Ω for $\beta = 0.4$ and $\delta = -0.25$. c) Bivariate transfer function T_L of the corresponding iso-τ line (red) of Figure 2a.

2.3. Distribution of particle characteristics

In the previous section we gave a stochastic description of CALs in the form of bivariate transfer functions T_L. On the other hand, particle mixtures themselves can be described by two-dimensional probability distributions, i.e., the relevant particle descriptors size d_p and mass density ρ_p of a particle mixture can be described by means of their joint probability distribution. More precisely, let (D, R) be a random vector consisting of size D and mass density R of a random particle. In many applications the distribution of the random vector (D, R) can be described by its two-dimensional probability density[3] $f\colon \mathbb{R}^2 \to [0, \infty)$ whose values have the unit m^2/kg, i.e., we assume that (D, R) is absolutely continuous. This allows us to derive various properties of particle mixtures, like for example the number-based fraction of particles in the mixture with size $d_\mathrm{p} \in [a, b]$ by computing

$$\mathbb{P}(D \in [a,b]) = \mathbb{P}((D,R) \in [a,b] \times \mathbb{R}) = \int_0^\infty \int_a^b f(d,\rho)\,\mathrm{d}d\,\mathrm{d}\rho. \tag{9}$$

The two-dimensional probability density f of mixtures of two types of dispersed particles, denoted by A and B, with number-based two-dimensional probability densities f_A and f_B, respectively, can then be modeled by

$$f(d,\rho) = \lambda f_A(d,\rho) + (1-\lambda) f_B(d,\rho), \tag{10}$$

where the parameter $\lambda \in [0, 1]$ describes the mixing ratio of particles of type A and B[4]. We make the assumption that particle characteristics are not correlated. However, note that the stochastic description introduced in the present paper does not require independence of particle size d_p and mass density ρ_p for the considered particle systems. Figure 3a depicts the probability density of a particle mixture of Cu and

[3] An absolutely continuous real-valued random variable X has a probability density $f_X\colon \mathbb{R} \to [0, \infty)$ such that the probability of the event that the values of X belong to some interval $[a, b] \subset \mathbb{R}$ is given by $\mathbb{P}(X \in [a, b]) = \int_a^b f_X(x)\,\mathrm{d}x$. Analogously, an absolutely continuous random vector $X = (X_1, X_2)$ has a probability density $f_X\colon \mathbb{R}^2 \to [0, \infty)$ such that $\mathbb{P}(X_1 \in [a_1, b_1], X_2 \in [a_2, b_2]) = \int_{a_1}^{b_1} \int_{a_2}^{b_2} f_X(x_1, x_2)\,\mathrm{d}x_2\mathrm{d}x_1$ holds (Jacod and Protter (2003); Karr (1993)). Note that the probability density f_X is normalized, i.e., $\int_{-\infty}^{\infty} \int_{-\infty}^{\infty} f_X(x_1, x_2)\,\mathrm{d}x_2\,\mathrm{d}x_1 = 1$ holds.

[4] The mixing ratio λ describes the mixture on the basis of particle numbers. Thus, the mass ratio of the mixture is in favor of the heavier particle species.

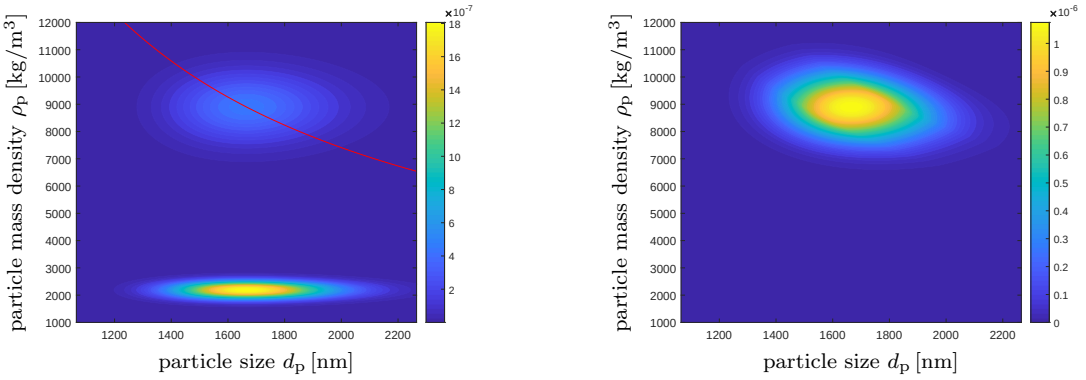

Figure 3. a) Two-dimensional probability density f of particle size-mass density vectors of an exemplary Cu-SiO_2 particle mixture. The red line is the iso-τ line of a CAL with lens parameters $p = 10\,\mathrm{Pa}$, $d_\mathrm{L} = 0.07\,\mathrm{m}$, $\dot{Q}_m = 0.02\,\mathrm{slm}$. b) The two-dimensional probability density $\widetilde{f}$ of size-mass density vectors of particles which pass through the CAL.

SiO_2 where the task of a CAL will be to separate the desired Cu particles from SiO_2 particles. Note that Figure 3a shows a bimodal probability density, where the mode centered at the mass density of $8900\,\mathrm{kg/m^3}$ originates from the Cu particles. The red line depicts an iso-τ line of a CAL. Since the iso-τ line does not pass through the mode of the probability density belonging to the SiO_2 particles, it can be expected that the separation task will be performed rather well.

2.4. Stochastic modeling of the separation process

We already mentioned that a CAL does not only separate particles whose size-mass density configurations $(d_\mathrm{p}, \rho_\mathrm{p})$ are located on the iso-τ line, but also particles whose size-mass density configurations are in the vicinity of this line. The bivariate transfer function T_L of a CAL takes this effect into account.

Using the bivariate transfer function T_L, we can compute the probability c_L that a particle, selected at random among all particles, with random size-mass density vector (D, R) passes through a CAL. For this purpose, we introduce an additional random variable U which is uniformly distributed on the unit interval $[0, 1]$ and stochastically independent of (D, R). Then, the probability of the event that the random particle passes the CAL is equal to the probability of the event that the inequality

$$T_\mathrm{L}(D, R) \geq U \tag{11}$$

holds. Note that for deterministic D and R the probability c_L of the event $T_\mathrm{L}(D, R) \geq U$ is the value of the transfer probability $T_\mathrm{L}(D, R)$ itself. On the other hand, for a random size-mass density vector (D, R) with joint density function f, this probability is given by

$$c_\mathrm{L} = \mathbb{P}(T_\mathrm{L}(D, R) \geq U) = \int_0^\infty \int_0^\infty f(d, \rho) T_\mathrm{L}(d, \rho)\,\mathrm{d}\rho\,\mathrm{d}d. \tag{12}$$

Moreover, it is possible to determine the two-dimensional probability density $\widetilde{f}$ of the vector $(\widetilde{D}, \widetilde{R})$, which describes the random size $\widetilde{D}$ and density $\widetilde{R}$ of those particles

which pass through the lens. The distribution of this random vector is equal to the conditional distribution of (D, R) under the condition that the random particle described by the vector (D, R) passes through the CAL. By computing the probability that the value of $(\widetilde{D}, \widetilde{R})$ belongs to a rectangle $C_1 \times C_2 \subset \mathbb{R}^2$, where $C_1, C_2 \subset \mathbb{R}^2$ are some given intervals, it is possible to determine the probability density $\widetilde{f}$ of $(\widetilde{D}, \widetilde{R})$. Namely, it holds that

$$\begin{aligned}\mathbb{P}(\widetilde{D} \in C_1, \widetilde{R} \in C_2) &= \mathbb{P}(D \in C_1, R \in C_2 \mid T_{\mathrm{L}}(D, R) \geq U) \\ &= \frac{1}{c_{\mathrm{L}}} \int_{C_1} \int_{C_2} f(d, \rho) T_{\mathrm{L}}(d, \rho) \, \mathrm{d}d \, \mathrm{d}\rho. \end{aligned} \tag{13}$$

Thus, the probability density $\widetilde{f}$ of the random size-mass density vector $(\widetilde{D}, \widetilde{R})$ of those particles which pass through the lens is given by

$$\widetilde{f}(d, \rho) = \frac{1}{c_{\mathrm{L}}} f(d, \rho) T_{\mathrm{L}}(d, \rho). \tag{14}$$

The conditional probability density $\widetilde{f}$ is visualized in Figure 3b for the input probability density f shown in Figure 3a.

2.5. Constraints on lens geometry and operating parameters

In the previous section we described the relative amount c_{L} of particles which pass through the CAL by Equation (12) and the probability density $\widetilde{f}$ of their particle characteristics in dependence of the CAL's bivariate transfer function T_{L}, see Equations (12) and (14), respectively. Since the bivariate transfer function T_{L} depends on the lens parameters $p, \dot{Q}_{\mathrm{m}}, d_{\mathrm{L}}$, see Equations (2), (3) and (8), we can modify the lens geometry and operating to influence the separation results. However, there are certain physical constraints on the lens parameters $p, \dot{Q}_{\mathrm{m}}, d_{\mathrm{L}}$ which we want to discuss in order to describe the space of valid parameter configurations. To reduce the complexity of the problem, the following deductions and assumptions are used:

(i) Particles do not affect the flow of the carrier gas.
(ii) The particle relaxation time is based on the pressure before passing the orifice[5].
(iii) All particles start in the same region of the lens, such that they experience the same velocity when going through the orifice.
(iv) Only subsonic and continuum flow conditions are considered.
(v) Particle mass load is small, to avoid coagulation which could change the size-distribution in the lens setup.

As stated in Wang et al. (2005) focusing of submicron particles is not possible when certain limits for Reynolds Re, Mach Ma and Knudsen Kn numbers are exceeded, where the limits are denoted by $\mathrm{Re}_{\mathrm{c}}, \mathrm{Ma}_{\mathrm{c}}$ and Kn_{c}, respectively. Additionally, the available pumping capacity is a further limiting factor. The equations for computing Re, Ma, Kn and their respective critical values given in Wang et al. (2005) are provided

[5]For CALs in use, mass flow rate of the carrier gas is fixed via mass flow control devices or critical orifices, thus the pressures in the CAL depend on the adjustable suction rate of the chosen pumping system. The pressure drop over the lens is small (< 10 Pa) in comparison to the pressure drop over the lens exits, and can be calculated.

below. The Reynolds number Re is calculated via the mass flow rate of the gas $\dot{Q}_\mathrm{m}$ by

$$\mathrm{Re} = \frac{\rho_\mathrm{g}(p) \cdot \bar{u} \cdot d_\mathrm{L}}{\mu_\mathrm{g}} = \frac{4 \cdot \dot{Q}_\mathrm{m}}{\pi \mu_\mathrm{g} d_\mathrm{L}} < 200 = \mathrm{Re_c}, \tag{15}$$

where μ_g is the gas viscosity. The Mach number Ma, given by

$$\mathrm{Ma} = \frac{u}{c_\mathrm{g}} < 1 = \mathrm{Ma_c}, \tag{16}$$

compares gas velocity u with the velocity of sound c_g in the gas. The Knudsen number Kn, which indicates whether a fluid flows as a continuum, is given by

$$\mathrm{Kn} = \frac{2 \cdot \lambda_\mathrm{g}(p)}{d_\mathrm{L}} < 0.1 = \mathrm{Kn_c}, \tag{17}$$

where λ_g is the mean free path of the gas.

The pumping capacity mentioned above limits the volume flow rate that can be pumped out of the system at a given pressure. There exists an optimal pressure for which the pump evacuates at a maximum volume flow rate. In the present paper we use measurements from a rotary vane pump (1001 Leybold) as exemplary data. More precisely, the function we use to describe the pressure-dependent volume pump rate S_slm in slm is given by

$$S_\mathrm{slm}(p) = 60 \cdot 10^{y(p)} \cdot \rho_\mathrm{g} \cdot (p/p_0) \cdot (T_0/T), \tag{18}$$

where $p_0 = 101325\,\mathrm{Pa}$ is the standard pressure, $T_0 = 273.15\,\mathrm{K}$ is the standard temperature and y denotes a polylogarithmic fit to the volume pump rate data provided in Leybold GmbH (2018) which is given by

$$y(p) = \sum_{k=0}^{8} x_k \log^k(p), \tag{19}$$

with fitted regression parameters

$$(x_0, x_1, \ldots, x_8) = (2.908, -0.016, -0.082, 0.050, 0.010, -0.025, -0.002, 0.006, -0.001).$$

Furthermore, the available pressure range is constrained by the pumping capacity:

$$10\mathrm{Pa} \leq p \leq 101325\mathrm{Pa}. \tag{20}$$

When we apply the constraints that result from the calculation of the critical values for $\mathrm{Re_c}$, $\mathrm{Ma_c}$, $\mathrm{Kn_c}$ and the pumping capacity, we can locate all feasible combinations of pressure, flow rate and lens diameter. Using Equation (3) we can calculate the values of τ_p belonging to the constrained parameter space. For every particle with mass density ρ_p and diameter d_p, there exists a surface, see Equation (4), in the 3D parameter space of pressure p, lens diameter d_L and mass flow $\dot{Q}_m$ such that the particle is optimally focused. Due to the constraints for the lens parameters given by Inequalities (15)-(17) and (20) the surface can be empty, but in our application there

are usually a multitude of combinations of p, d_{L} and $\dot{Q}_m$ which satisfy the constraints and for which the particle is optimally focused.

2.6. Performance measures

In Section 2.4 we described how to obtain the probability density $\widetilde{f}$ of size and mass density for feed particles which pass through a CAL with bivariate transfer function T_{L}. Since T_{L} depends on CAL operating parameters, the latter can be varied while respecting the constraints discussed in Section 2.5 in order to modify separation results. Therefore, we introduce quantities, which we refer to as performance measures, to evaluate the quality of a separation process. Furthermore, we derive some formulas which allow a quick numerical computation of performance measures. To do so, we analyze mass fractions in the feed, product and waste and differentiate between value and non-value materials. Figure 4 shows how these quantities are denoted: The mass fractions of the feed are labeled with the subscript F. Value material is labeled with v, while non-value material is labeled with nv. Thus, the mass m_{F} of the feed material consists of the mass $m_{v,\mathrm{F}}$ of the value material in the feed and the mass $m_{nv,\mathrm{F}}$ of the non-value material. The feed is separated in product and waste fractions denoted by P and W, respectively.

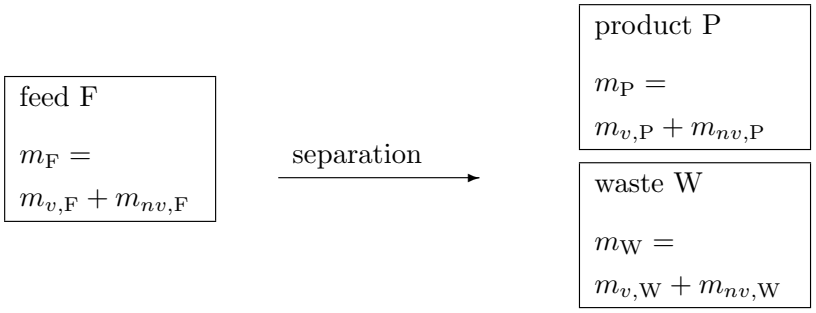

Figure 4. The feed F is separated into the product P and the waste W. Desired fractions are marked by v and undesired fractions by nv. The terms "product" and "waste" are used only to better distinguish the two separated fractions by name.

Furthermore, we consider the feed purity P_{F}, product purity P_{P} and product yield Y_{P} which are defined as follows:

$$P_{\mathrm{F}} = \frac{m_{v,\mathrm{F}}}{m_{\mathrm{F}}} = \frac{m_{v,\mathrm{F}}}{m_{nv,\mathrm{F}} + m_{v,\mathrm{F}}}, \tag{21}$$

$$P_{\mathrm{P}} = \frac{m_{v,\mathrm{P}}}{m_{\mathrm{P}}} = \frac{m_{v,\mathrm{P}}}{m_{nv,\mathrm{P}} + m_{v,\mathrm{P}}}, \tag{22}$$

$$Y_{\mathrm{P}} = \frac{m_{\mathrm{P}}}{m_{\mathrm{F}}} = \frac{m_{nv,\mathrm{P}} + m_{v,\mathrm{P}}}{m_{nv,\mathrm{F}} + m_{v,\mathrm{F}}}. \tag{23}$$

The ratio of product purity P_{P} divided by feed purity P_{F} describes the gain in

purity, or, in other words, the enrichment E of value material in the product P, i.e.,

$$E = \frac{P_{\mathrm{P}}}{P_{\mathrm{F}}}. \tag{24}$$

Multiplying the enrichment E with the product yield Y_P gives a measure for the yield of value material Y_v, i.e.,

$$Y_v = EY_{\mathrm{P}} = \frac{m_{v,\mathrm{P}}}{m_{v,\mathrm{F}}}. \tag{25}$$

In the present paper, we will quantify the separation performance by mainly considering the product yield Y_{P} and the yield of value material Y_v. These quantities are normalized and take values in the interval $[0, 1]$.

Having in mind the stochastic description of both the in-going particle mixtures and the CAL introduced in Sections 2.2 and 2.4, it is possible to estimate performance measures using Monte Carlo simulation (Asmussen and Glynn (2007); Kroese et al. (2013)). Therefore, for some $n > 1$, we consider the random vectors $(D_1, R_1), (D_2, R_2), \ldots, (D_n, R_n)$ with joint probability density f which represent n in-going random spherical particles. Note that the mass $m(D_i, R_i)$ of the i-th random particle described by the random size-mass density vector (D_i, R_i) is given by

$$m(D_i, R_i) = \frac{\pi}{6} D_i^3 R_i \tag{26}$$

for each $i = 1, \ldots, n$ and thus the (random) mass m_{F} of the n in-going random particles is given by

$$m_{\mathrm{F}} = \sum_{i=1}^{n} m(D_i, R_i) = \frac{\pi}{6} \sum_{i=1}^{n} D_i^3 R_i. \tag{27}$$

To decide whether the i-th random particle goes through the considered CAL with bivariate transfer function T_{L}, we consider an additional uniformly distributed random variable U_i on the unit interval $[0, 1]$. Recall that the particle passes the CAL if $U_i \leq T(D_i, R_i)$ holds, see Inequality (11). Thus, the (random) mass m_{P} of particles in the product is given by

$$m_{\mathrm{P}} = \frac{\pi}{6} \sum_{i=1}^{n} D_i^3 R_i \mathbb{1}_{U_i \leq T(D_i, R_i)}, \tag{28}$$

where $\mathbb{1}$ denotes the indicator function which is defined by

$$\mathbb{1}_{U_i \leq T(D_i, R_i)} = \begin{cases} 1, & \text{if } U_i \leq T(D_i, R_i), \\ 0, & \text{if } U_i > T(D_i, R_i). \end{cases}$$

To measure the separation performance we have to distinguish between spherical particles comprised of value and non-value materials. Therefore, we consider a predefined interval $C_v \subset (0, \infty)$, which describes the range of mass densities associated to the value material. Therefore, a random particle with size and density (D_i, R_i) is considered to be comprised of the value material if $R_i \in C_v$. With this definition of the value

material, we can formulate the mass $m_{v,\mathrm{F}}$ of value material in the feed as

$$m_{v,\mathrm{F}} = \frac{\pi}{6} \sum_{i=1}^{n} D_i^3 R_i \mathbb{1}_{R_i \in C_v}, \tag{29}$$

and, analogously, the mass $m_{v,\mathrm{P}}$ of value material in the product is given by

$$m_{v,\mathrm{P}} = \frac{\pi}{6} \sum_{i=1}^{n} D_i^3 R_i \mathbb{1}_{R_i \in C_v,\, U_i \leq T(D_i,R_i)}. \tag{30}$$

By inserting the formulas given in Equations (27) - (30) into the definitions considered in Equations (21) - (25) of our performance measures, we can estimate the separation performance. For instance, an estimator $\widehat{Y}_{\mathrm{P}}$ for the product yield Y_{P} is given by

$$\widehat{Y}_{\mathrm{P}} = \frac{\sum_{i=1}^{n} R_i D_i^3 \mathbb{1}_{U_i \leq T(D_i,R_i)}}{\sum_{i=1}^{n} R_i D_i^3}, \tag{31}$$

which can be computed via Monte Carlo simulation of the random vectors $(D_1, R_1), \ldots, (D_n, R_n)$. However, this approach can be relatively expensive, especially if the lens parameters $p, d_{\mathrm{L}}, \dot{Q}_m$ have to be optimized to maximize some performance measure, like the enrichment E, for a given distribution f of size-mass density vectors of incoming particles. To overcome this, we utilize the stochastic model of CALs described in Section 2.4, in order to derive theoretical formulas for the computation of performance measures in the case of an unboundedly increasing number n incoming random particles. Due to the law of large numbers (Jacod and Protter (2003); Karr (1993)) we have

$$\frac{1}{n} m_{\mathrm{F}} = \frac{1}{n} \sum_{i=1}^{n} m(D_i, R_i) \underset{n\to\infty}{\longrightarrow} \mathbb{E}\left[m(D,R)\right] = \int_0^\infty \int_0^\infty m(d,\rho) f(d,\rho)\, \mathrm{d}\rho\, \mathrm{d}d, \tag{32}$$

and, analogously,

$$\frac{1}{n} m_{\mathrm{P}} \underset{n\to\infty}{\longrightarrow} \mathbb{E}\left[m(D,R) \mathbb{1}_{T_{\mathrm{L}}(D,R) \geq U}\right] = \int_0^\infty \int_0^\infty m(d,\rho) f(d,\rho) T_{\mathrm{L}}(d,\rho)\, \mathrm{d}\rho\, \mathrm{d}d, \tag{33}$$

$$\frac{1}{n} m_{v,\mathrm{F}} \underset{n\to\infty}{\longrightarrow} \mathbb{E}\left[m(D,R) \mathbb{1}_{R \in C_v}\right] = \int_0^\infty \int_{C_v} m(d,\rho) f(d,\rho)\, \mathrm{d}\rho\, \mathrm{d}d, \tag{34}$$

$$\frac{1}{n} m_{v,\mathrm{P}} \underset{n\to\infty}{\longrightarrow} \mathbb{E}\left[m(D,R) \mathbb{1}_{T_{\mathrm{L}}(D,R) \geq U} \mathbb{1}_{R \in C_v}\right] = \int_0^\infty \int_{C_v} m(d,\rho) f(d,\rho) T_{\mathrm{L}}(d,\rho)\, \mathrm{d}\rho\, \mathrm{d}d, \tag{35}$$

where $\mathbb{E}$ denotes the expectation. Thus, the random variables considered in Equations (32) - (35) converge to deterministic limits. The integral representations of the limits in Equations (32) - (35) allow the numerical computation of the mass values of the feed and the product. Similarly, we can represent the limits of the separation performance

measures given in (21) - (25) via integrals. For example, the limit or, equivalently, the expected value of the product purity P_P for an unboundedly increasing number n of particles is given by

$$P_\mathrm{P} = \frac{m_{v,\mathrm{P}}}{m_\mathrm{P}} = \frac{\frac{1}{n} m_{v,\mathrm{P}}}{\frac{1}{n} m_\mathrm{P}} \to \frac{\int_0^\infty \int_{C_v} m(d,\rho) f(d,\rho) T_\mathrm{L}(d,\rho) \,\mathrm{d}\rho \,\mathrm{d}d}{\int_0^\infty \int_0^\infty m(d,\rho) f(d,\rho) T_\mathrm{L}(d,\rho) \,\mathrm{d}\rho \,\mathrm{d}d} = \mathbb{E}P_\mathrm{P}, \tag{36}$$

for $n \to \infty$. The expected values for the remaining performance measures can be derived analogously to (36). In the following, we will denote the expected values $\mathbb{E}P_\mathrm{F}, \mathbb{E}P_\mathrm{P}, \mathbb{E}Y_\mathrm{P}, \mathbb{E}E, \mathbb{E}Y_v$ simply by $P_\mathrm{F}, P_\mathrm{P}, Y_\mathrm{P}, E, Y_v$, respectively.

The formulas given in Equations (32) - (35) allow the numerical computation of expected performance measures for feed particle mixtures. More precisely, for any two-dimensional probability density f, which describes the number-based distribution of size-mass density of feed particles going through a CAL with bivariate transfer function T_L, we can numerically compute the measures $P_\mathrm{F}, P_\mathrm{P}, Y_\mathrm{P}, E$ and Y_v. By varying the lens parameters we can find suitable choices of operating parameters $p, d, \dot{Q}_m$ which optimize the separation quality with respect to one or several performance measures. In the following section we discuss this approach for various hypothetical separation problems.

3. Optimization of performance measures: A case study

In Section 2.6, we defined several quantities for measuring the separation performance of a CAL for mixtures having identical mean aerodynamic diameter and introduced analytical representations of these measures for numerical evaluation. Furthermore, in Section 2.5 we confined a reasonably sized space of viable operating parameters of a CAL. Thus, we can now conduct a case study for various distributions of feed particles, for which we search optimized initial parameters to be used later on in physical laboratory experiments.

3.1. Description of considered cases & approaches

Therefore, we consider various cases of particle mixtures which will be described by their joint probability density $f\colon \mathbb{R}^2 \to [0,\infty)$ as a function of size and mass density. For nanoparticles of one single type of material A with mean particle size d_A and mean mass density ρ_A such a joint probability density f_A will be modeled by

$$f_A(d,\rho) = f_1(d) f_2(\rho), \tag{37}$$

where f_1 is the probability density of a log-normal distribution with mean d_A and standard deviation[6] of 200 nm, which is truncated at 3000 nm such that only particle sizes below that threshold can occur. The function f_2 considered in (37) is the probability density of a normally distributed random variable with mean ρ_A and standard deviation $0.1\rho_A$, which is truncated such that only mass densities between 0

[6]The mean (or expectation) μ and standard deviation σ of a real-valued random variable X with probability density f are given by $\mu = \mathbb{E}X = \int_{-\infty}^{\infty} x f(x) \,\mathrm{d}x$ and $\sigma = \sqrt{\mathbb{E}\left[(X-\mu)^2\right]} = \left(\int_{-\infty}^{\infty} (x-\mu)^2 f(x) \,\mathrm{d}x\right)^{0.5}$, respectively (Jacod and Protter (2003); Karr (1993)).

Table 1. Feed properties of the considered cases including means of particle sizes and feed purities P_F. In each case both Cu and SiO_2 have the same mean aerodynamic diameter d_a.

cases	d_a [nm]	d_Cu [nm]	d_{SiO_2} [nm]	P_F [ ]
C1	500	168	307	0.82
C2	1000	335	614	0.68
C3	1500	503	921	0.62
C4	2000	670	1230	0.79

Table 2. Overview of approaches conducted in the case study.

A1	target mode of value material
A2a	optimize performance measure: Product purity
A2b	optimize performance measure: Product yield
A2c	optimize performance measure: Cost function
A3	second CAL for enhanced product yield

and $22\,000\,\mathrm{kg\,m^{-3}}$ can occur. Note that without truncating these distributions, physically unrealistic particles could occur. Furthermore, truncating distributions limits the range of integration in the formulas for the performance measures given in (27) - (30) to bounded sets, which in return makes numerical integration more viable. We also remark that in Equation (37) the particle size and mass density are modeled by stochastically independent random variables. On the other hand, note that it is possible to model such two-dimensional distributions for correlated particle size and mass density. For example the components $\exp\big(X_1\big)$ and X_2 of the random vector $(\exp\big(X_1\big), X_2)$ are log-normally and normally distributed and are in general correlated if (X_1, X_2) is a bivariate normally distributed random vector.

Recall that for mixtures of particles of type A and B with two-dimensional probability densities f_A and f_B, respectively, we can describe the joint density $f_{A,B}$ of such particle systems using the mixing ratio introduced in Equation (10). In the present paper we only consider the case $\lambda = 0.5$. Thus, the probability density $f_{A,B}$ models a particle mixture with equal numbers of particles of type A and B. However, this does not imply mass equality between particles of both types since their mass distributions can differ quite significantly.

In the present paper, we consider mixtures of Cu and SiO_2 particles as feed material, where we assume that Cu has a mean mass density of $\rho_\mathrm{Cu} = 8900\,\mathrm{kg\,m^{-3}}$ and SiO_2 has a mean mass density of $\rho_{\mathrm{SiO}_2} = 2190\,\mathrm{kg\,m^{-3}}$. In this case study we consider four different constellations, denoted by C1-C4, of mean particle sizes d_Cu and d_{SiO_2} which can be found in Table 1. Each case of volume equivalent diameters d_Cu and d_{SiO_2} corresponds, together with the mass densities $\rho_\mathrm{Cu}, \rho_{\mathrm{SiO}_2}$, to a respective aerodynamic diameter d_a, see Equation (5). Table 1 indicates that, for each particle size constellation C1-C4, the aerodynamic diameters d_a of Cu and SiO_2 particles are equal, which constitutes similar aerodynamic behavior of particles for a given constellation. For each of the considered cases the probability densities f_Cu and f_{SiO_2} of Cu and SiO_2 particles are assumed to have the form given in Equation (37). The joint probability densities $f_{\mathrm{Cu,SiO}_2}$ of characteristics of the mixtures are modeled by Equation (10), see Figure 5 (left column), with an equal (number-based) mixing ratio $\lambda = 0.5$. The corresponding resulting feed purities P_F are given in Table 1. For each of the considered feed materials C1-C4 we optimize the lens parameters $p, d_\mathrm{L}, \dot{Q}_m$ with respect to performance measures introduced in Section 2.6, on the basis of several approaches,

which will be denoted by A1, A2a, A2b, A2c and A3 in the following. For an overview of these approaches, see Table 2.

3.2. Target mode of value material (A1)

For each case stated in Table 1, lens parameters $p, d_{\mathrm{L}}, \dot{Q}_m$ are determined such that the constraints given in (15) - (17) and (20) are satisfied and the corresponding iso-τ line of the CAL goes through the mode of the probability density f_{Cu}. For each of the cases C1-C4, Figure 5 (left column, red line) shows the iso-τ lines of the CALs based on this approach. Heuristically speaking, this choice of the CAL parameters tries to maximize the number of Cu particles in the product P. However, this approach ignores the fact that larger particles carry more mass of value material which is reflected by the relatively low product yield Y_{P}, since it considers the mass of particles, see Table 3 (constellation C1). Moreover, the approach A1 does not try to minimize SiO_2 in the product which can lead to a low product purity P_{P}. Approach A1 serves as a reference to which the other approaches are compared to.

3.3. Optimize performance measures (A2)

In order to remedy the low product purity obtained by approach A1, we now choose CAL parameters, which maximize the product purity P_{P}, for each probability distribution $f_{\mathrm{Cu,SiO_2}}$ of feed material described by the cases C1-C4. This approach (denoted by A2a) is equivalent to maximizing the enrichment $E = \frac{P_{\mathrm{P}}}{P_{\mathrm{F}}}$, since the values of feed purity P_{F}, given in Table 1, do not depend on the CAL parameters.

To be more precise, for each feed material distribution $f_{\mathrm{Cu,SiO_2}}$ considered in C1-C4, we define a cost function $g_{\mathrm{A2a}} \colon D \to \mathbb{R}$, where $D \subset \mathbb{R}^3$ is the set of valid lens parameter constellations $(p, d_{\mathrm{L}}, \dot{Q}_m)$, i.e., $(p, d_{\mathrm{L}}, \dot{Q}_m) \in D$ if and only if $(p, d_{\mathrm{L}}, \dot{Q}_m)$ satisfies the constraints given by (15)-(17) and (20). The values of the cost function are given by

$$g_{\mathrm{A2a}}(p, d_{\mathrm{L}}, \dot{Q}_m) = -E(p, d_{\mathrm{L}}, \dot{Q}_m), \tag{38}$$

where $E(p, d_{\mathrm{L}}, \dot{Q}_m)$ is the enrichment E obtained by a CAL with parameters $p, d_{\mathrm{L}}, \dot{Q}_m$ for the feed material distribution $f_{\mathrm{Cu,SiO_2}}$. Note that the performance measure $E(p, d_{\mathrm{L}}, \dot{Q}_m)$ can be computed numerically using the integral representation introduced in Section 2.6. The optimal parameter constellation $(p_{\mathrm{opt}}, d_{\mathrm{L,opt}}, \dot{Q}_{m,\mathrm{opt}})$ of the CAL minimizes the cost function g_{A2a} (thus maximizes the enrichment E) and is given by

$$(p_{\mathrm{opt}}, d_{\mathrm{L,opt}}, \dot{Q}_{m,\mathrm{opt}}) = \operatorname*{argmin}_{(p,d_{\mathrm{L}},\dot{Q}_m)\in D} g_{\mathrm{A2a}}(p, d_{\mathrm{L}}, \dot{Q}_m). \tag{39}$$

This constrained optimization was performed using the particle swarm optimization algorithm in Matlab, see Eberhart and Kennedy (1995) and Mezura-Montes and Coello (2011), which, however, does not necessarily provide a global minimum. The CAL parameters determined in this way are given in Table 3 and the corresponding values of the performance measures $Y_{\mathrm{P}}, P_{\mathrm{P}}$ are listed in Table 3. In comparison to the results obtained by approach A1, the product purity increased significantly. However, this optimization can lead to a rather poor yield, see, for example, case C1. This is due to the fact that the maximization of the enrichment would be achieved if the CAL would

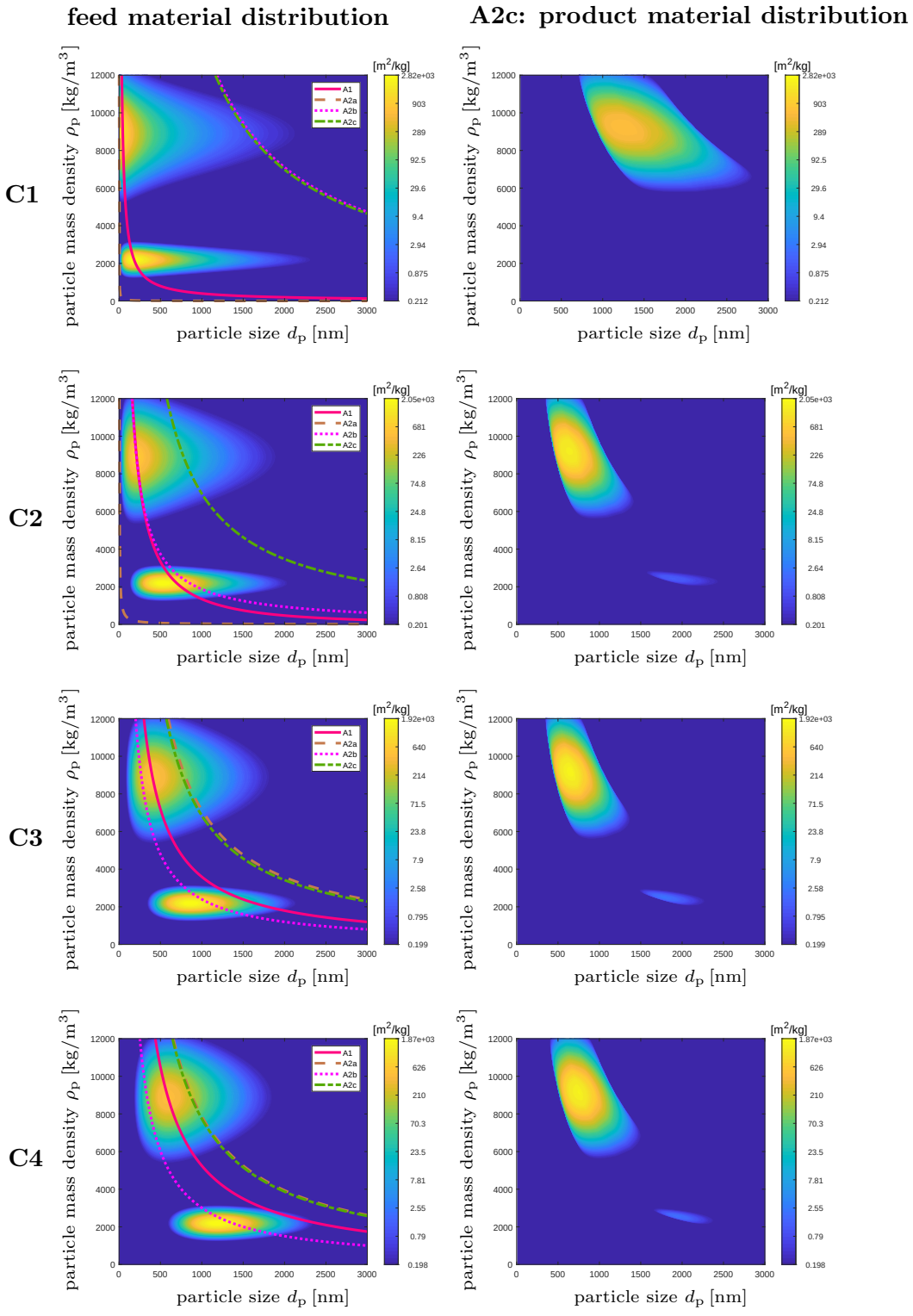

Figure 5. Left column: probability densities f of the Cu-SiO_2 particle mixtures in feed of cases C1-C4. The lines indicate the iso-τ lines of CALs optimized with the approaches A1, A2a, A2b and A2c, respectively. Right column: probability density $\widetilde{f}$ of the feed material considered in C1-C4 after passing through a CAL which was optimized using approach A2c.

solely separate one single particle comprised of the value material.

On the other hand, if we chose the following cost function: $g_{\mathrm{A2b}}(p, d_{\mathrm{L}}, \dot{Q}_m) = -Y_{\mathrm{P}}(p, d_{\mathrm{L}}, \dot{Q}_m)$, which optimizes the product yield P_{P} (approach A2b), the product purity can suffer, see case C4 in Table 3.

Therefore, neither the optimization of the product purity P_{P} nor the product yield Y_{P} seem to be suitable as possible goals. As an alternative approach (A2c) we thus propose the cost function $g_{\mathrm{A2c}}(p, d_{\mathrm{L}}, \dot{Q}_m) = -Y_v(p, d_{\mathrm{L}}, \dot{Q}_m)E(p, d_{\mathrm{L}}, \dot{Q}_m)$. This approach tries to maximize both the yield of the value material Y_v and the enrichment E. Note that the best separation result would be achieved if the CAL would separate the entire fraction of the value material (maximizes Y_v), but moreover, if it only separates the value material (maximizes E). In comparison to the previously described approaches A1, A2a and A2b, the maximization of both the yield of value material Y_v and the enrichment E leads to a good compromise between purity and yield, see Table 3. The probability densities corresponding to the products of cases C1-C4 obtained by approach A2c are visualized in Figure 5 (right column).

The iso-τ lines obtained with the optimization approaches A2a, A2b and A2c are also depicted depicted in Figure 5 (left column). It indicates that the iso-τ lines obtained by the optimization approaches A2a and A2c avoid the mode of SiO_2 particles in the feed distributions. This is due to the fact that the cost functions in both approaches consider the enrichment E. However, as it can be seen for the cases C1 and C2, the approach A2a sometimes provides iso-τ lines indicating a separation of rather small Cu particles which leads to a poor product yield. Approach A2b, which solely maximizes the product yield Y_{P}, often leads to iso-*tau* lines, see cases C2-C4, which do not avoid the mode corresponding to the non-value SiO_2 particles. On the other hand, the iso-τ lines obtained by approach A2c avoid the mode corresponding to SiO_2 particles and indicate separation of relatively large particles which leads to both a good product purity P_{P} and product yield Y_{P}.

3.4. Utilize a second CAL (A3)

Even though approach A2c leads to good results, Table 3 indicates a relatively low product yield. Note that a high yield Y_{P} is not necessarily desired, since this could mean that no separation at all took place. However, it is still possible to increase the product yield while maintaining a good purity by introducing a second CAL, which extracts value material from the waste of the first CAL.

Figure 6 visualizes this procedure, denoted by approach A3, for case C1. Note that, similarly to a system of just one CAL, we can derive formulas for performance measures of such a system with two CALs, which measure the quality of the two separated fractions. Therefore, it is possible to optimize both the lens parameters of the first and second lens, which improves the separation performance even further, see Table 3. For example, for the case C1 the product yield improved from 0.12 to 0.21 while maintaining a purity of 0.96.

4. Results & conclusions

4.1. Results

The results given in Table 3 show some trends. For instance, when comparing the product yield Y_{P} of the considered cases, it is found that a greater value of the aerody-

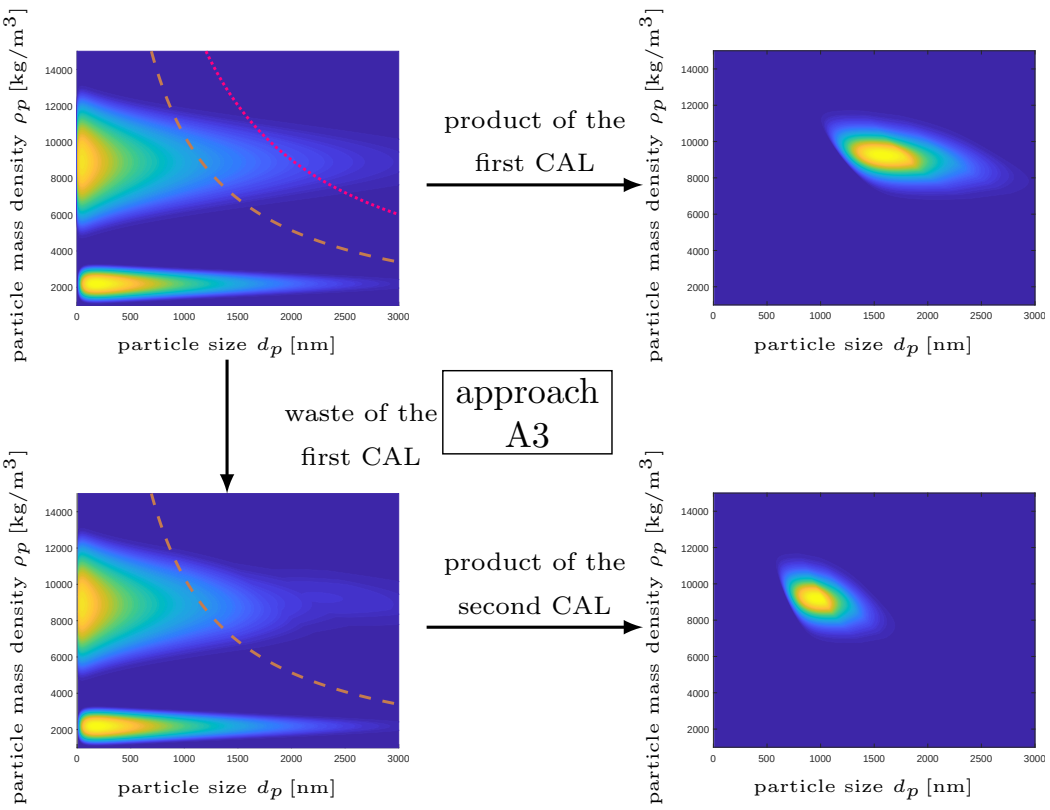

Figure 6. Scheme for improving the product yield by introducing a second CAL which separates the waste fraction of the first CAL (approach A3). Top left: probability density of a Cu and SiO_2 particle mixture of case C1 (logarithmic color scale). The red and brown lines indicate iso-τ lines of the first and second CAL, respectively. Top right: probability density of the fraction separated by the first CAL. Bottom left: probability density of the waste fraction of the first CAL (logarithmic color scale). The brown line indicates the iso-τ line of the second CAL. Bottom right: probability density of the separated fraction after the waste of the first CAL passed through the second CAL.

Table 3. Optimized CAL parameters and computed performance measures Y_P and P_P for the feed materials C1-C4 and the approaches A1-A3.

Case	Approach	p [Pa]	d_L [mm]	$\dot{Q}_\mathrm{m}$ [slm]	Y_P	P_P
C1: $d_\mathrm{a} = 500$ nm	A1	10	100	3	0.004	0.025
	A2a	10	24.3	3.25	6.6e-16	0.98
	A2b	10	23.1	0.001	0.12	0.96
	A2c	10	23.1	0.001	0.12	0.96
	A3	10/375	25.0/10.0	0.001/0.153	0.22	0.96
C2: $d_\mathrm{a} = 1000$ nm	A1	42.8	100	11.2	0.15	0.067
	A2a	10	35.0	1.38	1.4e-19	0.98
	A2b	10	56.2	0.110	0.15	0.065
	A2c	11	18.4	0.0011	0.11	0.96
	A3	10/183	17.4/21.1	0.001/0.396	0.2	0.95
C3: $d_\mathrm{a} = 1500$ nm	A1	10	100	0.32	0.13	0.34
	A2a	10	18.9	0.0011	0.13	0.96
	A2b	10.6	70.0	0.185	0.22	0.031
	A2c	10	18.2	0.001	0.13	0.96
	A3	10/237	19.5/20.5	0.001/0.952	0.22	0.95
C4: $d_\mathrm{a} = 2000$ nm	A1	10	17	0.001	0.11	0.72
	A2a	10	19.0	0.001	0.15	0.96
	A2b	10	14.9	0.0013	0.26	0.014
	A2c	10.4	18.8	0.0011	0.15	0.96
	A3	10/320	18.7/17.5	0.001/0.691	0.23	0.95

namic diameter is linked to a higher product yield. An explanation for this is that the performance measure is biased towards mass, and particle mass is strongly influenced by the particle size. This bias can be seen in the product purity P_P as well, but it is not nearly as pronounced as in the product yield Y_P. In general, the more complex approaches A3/A2c lead to better performance than the approaches which target the mode (A1) or optimize a single performance measure (A2a and A2b). Another observation is that the cost function introduced in approach A2c favors the product purity over the product yield. An interesting quality emerges when comparing the optimized parameter sets of different approaches: They display remarkable similarity and seem to approach the boundary of the parameter space. Almost all of the optimized parameter combinations have values close to the lower constraint for the pressure which is given by 10Pa, see Inequality (20). The tendency to low pressure values is no surprise because for lower pressures the Cu and SiO_2 particles become less similar aerodynamically. This is due to the difference in the particle slip, which depends only on particle size but not on the mass density. Due to limitations of pumping capacity, the low pressure reduces the maximum mass flow rate which the system is able to handle. This is problematic, because we intuitively expected that one optimized parameter set would be found between pressure values from 100 to 1000 Pa, because this domain inhabits the highest pumping capacities. Thus, making higher mass flow rates possible, which should in turn lead to higher product yield, given that the mass load - the mass of particles per volume of gas flow - stays equal. But surprisingly this expected trend is not really found in the simulations.

4.2. Conclusions

Classifying aerodynamic lenses offer an adjustable, differential transfer function which enables them to separate particles by size and mass density. Stochastic modeling provides a highly adjustable tool for choosing the best preconditions in a design process.

For the goal of aerodynamic classification, it was possible to make reasonable predictions regarding the influence of various process parameters on the separation performance. These predictions reduce the risks that can occur while making certain design decisions. Therefore, we introduced different quantities for measuring the separation performance, such that it was possible to analyze and optimize the performance of the separation process. These performance measures are applicable for different forms of separation processes and are based on practicability.

We selected a few interesting virtual particle mixtures for a case study, namely mixtures of Cu and SiO_2, for which the valuable Cu particles should be extracted. For these particle systems, the CAL geometry and the operating parameters were optimized with respect to several performance measures in order to obtain large quantities of pure separation products. We have seen that some particle mixtures are rather easy to separate while others are more challenging in this regard. When the design parameters are carefully chosen, yield and purity are improved by two to three orders of magnitude. Additionally, it is possible to further enhance the separation performance, by repeating the separation process on the waste of the first CAL (in order to improve the product yield).

The described methods can be easily transferred to different separation processes, for which the influence of process parameters on the transfer functions are well understood. Then, process parameters can be optimized with respect to performance measures for arbitrary feed materials.

List of Symbols

Symbol	Dimension	Description
m	[kg]	mass
d_p	[m]	volume equivalent particle diameter
τ_p	[s]	particle relaxation time
ρ_p	[kg/m^3]	particle mass density
d_L	[m]	orifice diameter
τ_L	[s]	lens relaxation time
l	[m]	length
ρ_g	[kg/m^3]	gas density
ρ_0	[kg/m^3]	unity density
λ_g	[m]	gas mean free path
η_g	[Pa·s]	dynamic gas viscosity
u_g	[m/s]	mean gas velocity
C_C		Cunningham correction
$\dot{Q}m$	[kg/s]	gas mass flow rate
$\dot{Q}_\mathrm{v}$	[m^3/s]	gas volume flow rate
$\dot{Q}_\mathrm{slm}$	[slm]	volume flow rate in standard litre per minute

S	$[\mathrm{m}^3/\mathrm{s}]$	pumping speed
p	[Pa]	pressure
T	[K]	temperature
Stk		Stokes number
Re		Reynolds number
Ma		Mach number
Kn		Knudsen number
Y		yield
P		purity
E		enrichment
$\mathbb{1}$		indicator function
f		probability density function
$\mathbb{P}$		probability measure
$\mathbb{E}$		expectation
D		random volume equivalent particle diameter
R		random mass density
λ		mixing ratio of particle species

Index	**Description**
$_{\mathrm{a}}$	aerodynamic
$_{\mathrm{p}}$	particle
$_{\mathrm{L}}$	lens
$_{\mathrm{g}}$	gas
$_{\mathrm{c}}$	critical
$_{\mathrm{o}}$	optimal
$_{0}$	standard conditions
$_{\mathrm{F}}$	feed
$_{\mathrm{P}}$	product
$_{\mathrm{W}}$	waste

Acknowledgments

We would like to thank "Deutsche Forschungsgemeinschaft" (DFG) for financially supporting this research project (grants KR1723/19-1 and SCHM997/27-1) within SPP 2045.

References

Asmussen, S. and Glynn, P. W. (2007). *Stochastic Simulation: Algorithms and Analysis*. Springer, New York.

Babick, F., Hillemann, L., Stintz, M., Dillenburger, T., Pitz, M., Hellmann, A., Antonyuk, S., Ripperger, S., Huber, F. J. T., Will, S., Wernet, R., Seipenbusch, M., Gensch, M., Weber, A., Kiesler, D., Kruis, E., Friehmelt, R., and Sachweh, B. (2018). Multiparameter characterization of aerosols. *Chemie Ingenieur Technik*, 90(7):923–936.

de La Mora, J. F. and Riesco-Chueca, P. (1988). Aerodynamic focusing of particles in a carrier gas. *Journal of Fluid Mechanics*, 195:1–21.

Dong, Y., Bapat, A., Hilchie, S., Kortshagen, U., and Campbell, S. A. (2004). Generation of nano-sized free standing single crystal silicon particles. *Journal of Vacuum Science and Technology B: Microelectronics and Nanometer Structures*, 22(4):1923–1930.

Drewnick, F., Hings, S. S., DeCarlo, P., Jayne, J. T., Gonin, M., Fuhrer, K., Weimer, S., Jimenez, J. L., Demerjian, K. L., Borrmann, S., and Worsnop, D. R. (2005). A new time-of-flight aerosol mass spectrometer (TOF-AMS) - Instrument description and first field deployment. *Aerosol Science and Technology*, 39(7):637–658.

Eberhart, R. and Kennedy, J. (1995). Particle swarm optimization. In *Proceedings of the IEEE International Conference on Neural Networks*, volume 4, pages 1942–1948. Citeseer.

Friedlander, S. K. (2000). *Smoke, Dust, and Haze*. Topics in Chemical Engineering. Oxford University Press, Oxford, 2nd edition.

Jacod, J. and Protter, P. (2003). *Probability Essentials*. Springer, Berlin.

Karr, A. F. (1993). *Probability*. Springer, New York.

Kiesler, D., Bastuck, T., Kennedy, M. K., and Kruis, F. E. (2019). Development of a high flow rate aerodynamic lens system for inclusion of nanoparticles into growing pvd films to form nanocomposite thin films. *Aerosol Science and Technology*, 54(54):1–17.

Klimešová, E., Kulyk, O., Gu, Y., Dittrich, L., Korn, G., Hajdu, J., Krikunova, M., and Andreasson, J. (2019). Plasma channel formation in NIR laser-irradiated carrier gas from an aerosol nanoparticle injector. *Scientific Reports*, 9(1):8851.

Kroese, D. P., Taimre, T., and Botev, Z. I. (2013). *Handbook of Monte Carlo Methods*, volume 706. J. Wiley & Sons, Hoboken, New Jersey.

Leybold GmbH (2018). Ruvac roots vacuum pumps: Excerpt from the Leybold full line catalog 2018, catalog part: Roots vacuum pumps.

Liu, P., Ziemann, P. J., Kittelson, D. B., and McMurry, P. H. (1995). Generating particle beams of controlled dimensions and divergence. *Aerosol Science and Technology*, 22:314–324.

Mallina, R. V., Wexler, A. S., and Johnston, M. V. (1999). High-speed particle beam generation. *Aerosol Science & Technology*, 30:719–738.

Mezura-Montes, E. and Coello, C. A. C. (2011). Constraint-handling in nature-inspired numerical optimization: past, present and future. *Swarm and Evolutionary Computation*, 1(4):173–194.

Piseri, P., Tafreshi, H. V., and Milani, P. (2004). Manipulation of nanoparticles in supersonic beams for the production of nanostructured materials. *Current Opinion in Solid State and Materials Science*, 8(3-4):195–202.

Rao, N. P., Navascues, J., and La Fernández de Mora, J. (1993). Aerodynamic focusing of particles in viscous jets. *Journal of Aerosol Science*, 24:879–892.

Schreiner, J., Schild, U., Voigt, C., and Mauersberger, K. (1999). Focusing of aerosols into a particle beam at pressures from 10 to 150 torr. *Aerosol Science and Technology*, 31(5):373–382.

Stolzenburg, M. R. and McMurry, P. H. (2008). Equations governing single and tandem dma configurations and a new lognormal approximation to the transfer function. *Aerosol Science and Technology*, 42:421–432.

Wang, X., Kruis, F. E., and McMurry, P. H. (2005). Aerodynamic focusing of nanoparticles. *Aerosol Science and Technology*, 39:611–623.

Wang, X. and McMurry, P. H. (2006). A design tool for aerodynamic lens systems. *Aerosol Science and Technology*, 40:320–334.

Willeke, K., editor (2011). *Aerosol Measurement: Principles, Techniques, and Applications: Third Edition*. J. Wiley & Sons, Hoboken, New Jersey.

Zhang, X., Smith, K. A., Worsnop, D. R., Jimenez, J. L., Jayne, J. T., and Kolb, C. E. (2002). A numerical characterization of particle beam collimation by an aerodynamic lens-nozzle system: Part I. an individual lens or nozzle. *Aerosol Science and Technology*, 36:617–631.